TRACKING RAPID INTRACELLULAR MOVEMENTS: A BAYESIAN RANDOM SET APPROACH

BY VASILEIOS MAROULAS AND ANDREAS NEBENFÜHR[1]

University of Tennessee

We focus on the biological problem of tracking organelles as they move through cells. In the past, most intracellular movements were recorded manually, however, the results are too incomplete to capture the full complexity of organelle motions. An automated tracking algorithm promises to provide a complete analysis of noisy microscopy data. In this paper, we adopt statistical techniques from a Bayesian random set point of view. Instead of considering each individual organelle, we examine a random set whose members are the organelle states and we establish a Bayesian filtering algorithm involving such set states. The propagated multi-object densities are approximated using a Gaussian mixture scheme. Our algorithm is applied to synthetic and experimental data.

1. Introduction. Most plant cells display a striking phenomenon called "cytoplasmic streaming," a process that has been recognized since the late 18th century by Corti (1774). During cytoplasmic streaming, most subcellular organelles move rapidly through the cell, resulting in constant mixing of the soluble components of the cytoplasm. The function of these movements is not known, although a potential role in better distribution of metabolites has been proposed in Shimmen and Yokota (1994). The movements are driven by myosin motor proteins [Shimmen (2007)] and appear to be necessary for normal growth of plant cells and ultimately the whole plant [Ojangu et al. (2012), Peremyslov et al. (2008)]. The molecular mechanisms that connect the intracellular movements with cell growth are not known [Madison and Nebenführ (2013)]. Better understanding of these cellular processes requires the targeted manipulation of the movements followed by quantitative assessment of the resulting changes at the subcellular, cellular and whole-plant levels. Recent results have identified additional regulatory mechanisms that influence intracellular movements, although the precise nature of these mechanisms is still unknown [Vick and Nebenführ (2012)]. This is due, at least in part, to the astounding complexity of these movements and the technical difficulty of describing them accurately [Hamada et al. (2012), Nebenführ et al. (1999)].

Recent advances in molecular biology and fluorescence microscopy imaging have made possible the detailed observation of these intracellular dynamics and the acquisition of large multidimensional image data sets [Danuser (2011)]. Paredez, Somerville and Ehrhardt (2006) noted that these time-lapse observations reveal a large number of nearly identical particles that move with high velocities in close proximity to each other. Combined with the saltatory, or stop-and-go, nature of their motions, these features make automated tracking of these movements an extremely difficult task as discussed in Nebenführ et al. (1999). As a result, most previous analyses have relied on manual tracking of a few individual particles, for example, Collings et al. (2002), Gutierrez et al. (2009), Hamada et al. (2012), Logan and Leaver (2000), Nebenführ et al. (1999). A full understanding of the observations, however, requires accurate tracking of a large number of bright spots in noisy image sequences, which can be accomplished only by an automated algorithm that is able to analyze the data completely [Danuser (2011)]. This complete analysis will require reliable identification of organelle positions (coordinates) from the bright spots in fluorescent microscope images taken at different times and the correct linking of these positions into continuous movement trajectories over all time points. One benefit of such an algorithm could be the emergence of recurring patterns such as the recent discovery, based on manual tracking, that organelles preferentially pause their motions at microtubules [Hamada et al. (2012)]. Thus, it seems likely that a comprehensive and accurate tracking algorithm will unearth additional regulatory events that in turn can be studied experimentally. Moreover, from a statistical point of view, an automated tracking algorithm will reduce the bias since manual tracking depends solely on experts' decision of linking the positions of bright spots at subsequent time points.

Mathematical and statistical models that require knowledge from statistics, probability, scientific computing and statistical mechanics have been developed for reliably tracking multiple objects in space. There are a great number of studies addressing the problem of tracking multiple targets in various settings. A partial list of such works is Bar-Shalom and Blair (2000), Blackman and Popoli (1999), Doucet, de Freitas and Gordon (2001), Fortmann, Bar-Shalom and Scheffe (1983), Gilks and Berzuini (2001), Goodman, Mahler and Nguyen (1997), Liu (2008), Liu and Chen (1998), Maroulas and Stinis (2012), Vo, Vo and Cantoni (2007), Mahler (2007, 2003), Mahler and Maroulas (2013). However, only a small number of multi-object models have been considered for specific microscopy image data, for example, Jaqaman et al. (2008), Sbalzarini and Koumoutsakos (2005), Smal (2009), Smal, Niessen and Meijering (2006). Movement of subcellular particles in living cells poses a highly complex problem for automated tracking algorithms. Even at high magnification, the true position of a particle within a cell can be only measured to within 50–200 nm due to limitations in optical resolution, and given the inevitable image noise, it is likely that some organelles are not detected. Moreover, not only can individual organelles move independently,

they also can change their behavior rapidly, their paths are not static, and organelles in close proximity can display strikingly different behaviors [Collings et al. (2002), Nebenführ et al. (1999)]. Commercial automated tracking algorithms such as Perkin–Elmer's "Volocity" were sometimes used to gain insights into overall movement patterns or derive average movement velocities; for example, see Avisar et al. (2008), Peremyslov et al. (2008). However, these algorithms often introduced mis-assignments in the tracks [e.g., Figure 3A in Avisar et al. (2008)] and, therefore, cannot be used to obtain an accurate global view of organelle motility.

In general, from a statistical point of view, tracking of multiple objects is an inherently difficult problem and consists of computing the best estimate of the objects' trajectories based on noisy observations. The estimates are propagated by a posterior distribution which considers organelles' dynamics and combines them with data. The greater the number of objects that are being tracked, the more complicated the tracking algorithm becomes. There are several techniques, for example, Kalman filters and their derivatives, particle filters, for addressing this problem statistically. The reader may refer to Gordon, Salmond and Smith (1993), Liu (2008) and the references therein.

A popular approach to tracking is particle filtering. Smal et al. (2008) introduced a particle filtering algorithm for the tracking problem using microtubule dynamics, which overall follow a priori known and fairly straight paths and can therefore be conveniently modeled. In general, the particle filter approach is an importance sampling method which approximates the posterior distribution by a discrete set of weighted samples (particles). However, it is often found in practice that most samples' contribution to the posterior distribution will be negligible. Therefore, carrying them along does not contribute significantly to finding an estimate. Hence, one may resample the particles to create more copies of samples with significant weights [Gordon, Salmond and Smith (1993)]. However, even with the resampling step, the particle filter might still need a large number of samples in order to approximate accurately the target distribution. Typically, a few samples dominate the weight distribution, while the rest of the samples are in statistically insignificant regions [Snyder et al. (2008)]. Thus, some studies [see, e.g., Gilks and Berzuini (2001), Kang and Maroulas (2013), Maroulas and Stinis (2012), Weare (2009)] have used an additional Markov Chain Monte Carlo step which helps to move more samples into statistically significant regions and thus to improve the diversity of samples. This extra step can improve estimates for multi-target tracking scenarios [Kang, Maroulas and Schizas (2014), Maroulas and Stinis (2012)], but at the price of adding an additional layer of complexity.

In this manuscript, we attempt to avoid the technical algorithmic steps which depend on the specific nature of different applications. Instead, we create an automated statistical tracking algorithm for independently evolving intracellular movements by considering a pertinent multi-object statistical framework. This framework adopts a Bayesian random set filtering technique. The key innovation in our approach is to conceptually view the evolving collection of organelles as a

single set-valued state and the collection of the experimental measurements as a single set-valued observation. A set-valued state contains not only the position of existing organelles but also the states of new biological entities which enter the tracking domain. Using Random Finite Set (RFS) theory and modeling the collection of organelles and their corresponding experimental measurements as sets result in *generalizing single-object filtering to a rigorous formulation of Bayesian multi-object filtering*. Multi-object filtering, similar to the single-object case, consists of two stages, the prediction stage using modeled or experimentally derived dynamics, and the update stage using the observed data. Both these steps involve multi-object distributions which lead to the multi-object Bayesian filtering posterior distribution,

$$f(X|Z_1, \ldots, Z_t) \propto f(Z_t|X) f(X|Z_1, \ldots, Z_{t-1}),$$

where $X, Z_1, \ldots, Z_t$ are appropriate random sets, formally defined in Section 2.

The general multi-object Bayes filtering distribution, $f(X|Z_1, \ldots, Z_t)$, is, however, computationally intractable in most applications and thus it needs to be approximated. In this paper, we consider a Gaussian mixture Cardinalized Probability Hypothesis Density (CPHD) approximation. The CPHD, first introduced by Mahler (2007), propagates two estimates, the cardinality distribution of a random set which yields an estimate of the number of objects per time step, and the intensity of a random finite set or otherwise the so-called probability hypothesis density (PHD) [Mahler (2003)]. The PHD is similar to the first-moment density or intensity density in point process theory; for example, see Daley and Vere-Jones (1988). The PHD first monitors multiple objects as clusters, and then attempts to resolve individual objects only as the quality and quantity of data permits. One could also estimate the number of objects at a given time step using the PHD, however, such an estimate is unstable when the experimental scene is highly dynamic, that is, with rapid entry and exit of organelles from the region of interest. A Gaussian mixture approximation of the CPHD was introduced by Vo, Vo and Cantoni (2007) whose algorithmic complexity was of the order $\mathcal{O}(m^3 n)$, where m is the number of data points (acquired positions of organelles) and n the true number of objects of interest. However, the cubic dependency on the number of data points is disadvantageous for our biological framework due to their large number.

In our manuscript, we consider a Gaussian mixture CPHD based on the experimental fact that data are generated only when organelles are present in the tracking domain. A false alarm is generated in signal detection when a nontarget event exceeds the detection threshold. Our experiments did not suffer from any false alarm, and thus a pertinent approximation of the CPHD is established in Propositions 2.1 and 2.2. The associated algorithmic implementation cost reduces to the order of $\mathcal{O}(mn)$, that is, the cost is linear with respect to the number of data and organelles. In brief, Proposition 2.1 propagates the predicted cardinality and the predicted intensity estimate (PHD) of a random finite set which follows a

Gaussian mixture density. Taking into consideration a new random set of data (positions of organelles), Proposition 2.2 updates the two predictions by considering a Bayesian set formulation. The posterior PHD follows an appropriate Gaussian mixture whose components are derived with the aid of Proposition 2.2.

A similar algorithm was analyzed in Mahler and Maroulas (2013) for the special case of monitoring two fixed objects that spawn several objects along their ballistic trajectories. These secondary objects fall under gravity, and thus they are not of tracking interest. Precisely, a distance criterion was computed to distinguish the two primary objects from the spawned ones. When this distance exceeded a certain threshold, the corresponding objects were declared debris and they were discarded. This assumption cannot be incorporated herein. Thus, in our framework, we relax this condition and, moreover, we incorporate several experimental biophysical features to understand the unknown dynamics of organelles. For instance, based on the organelles' acceleration data analysis (see Section 3), we discover that the acceleration follows a normal distribution with mean-zero. Assuming that the mass of the observed organelles did not change significantly between individual images (a valid assumption), we are able to deduce interesting results about the developed biomechanics within a cell.

Section 2 focuses on the methodology that was followed to establish an automated tracking algorithm for organelle movement data. Definitions of the Cardinalized Probability Hypothesis Density (CPHD) and approximation schemes are also presented. Section 3 describes the implementation of an appropriate version of the Gaussian mixture CPHD filter suited for the biological data (synthetic and experimental). Section 3.2 describes the biophysical conditions under which the experimental data were collected and the process of manual tracking. Finally, our results are summarized in Section 4 and a discussion for future research and developments is offered.

2. Random finite sets and approximations. We motivate this section by considering first the problem of tracking only one object. Suppose that an organelle, whose state is x' at time t, moves following the dynamics below,

$$(2.1) \qquad x_{t+1} = \phi_t(x', u_t),$$

where u_t is a randomly distributed noise and $\phi_t : \mathbb{R}^N \times \mathbb{R}^N \to \mathbb{R}^N$ is a family of nonlinear, nonsingular functions. Let $z_{1:t} \doteq \{z_1, z_2, \ldots, z_t\}$ denote the data history up to time t and let $f_{t|t}(x'|z_{1:t})$ represent the posterior probability density function (p.d.f.) at a given time t. Furthermore, consider the posterior predictive p.d.f., $f_{t+1|t}(x|z_{1:t})$, which merely yields the probability that an organelle will move to state x at time $t+1$ given the available data $z_{1:t}$. Using the Chapman–Kolmogorov equation, the posterior predictive distribution is given by

$$(2.2) \qquad f_{t+1|t}(x|z_{1:t}) = \int f_{t+1|t}(x|x') f_{t|t}(x'|z_{1:t}) \, dx',$$

where $f_{t+1|t}(x|x')$ is the Markov transition density associated with the dynamics expressed of equation (2.1). At given time $t + 1$, a new microscopy observation is collected, $z_{t+1} \in \mathbb{R}^M$. Typically, the dimension of organelle states, N, and the dimension of data, M, are not identical, $N \neq M$. For example, the state of organelles involves their position on the xy-plane and the corresponding velocities, that is, $N = 4$, whereas only the positions ($M = 2$) are available from the experimental data. The prediction (2.2) needs to be updated using the datum z_{t+1}. The collected measurement is a function of the true organelle's state perturbed by noise, that is,

$$(2.3) \qquad z_{t+1} = \eta_{t+1}(x, \xi_{t+1}),$$

where ξ_{t+1} is a randomly distributed noise, independent from v_t, and the function $\eta_{t+1} : \mathbb{R}^N \times \mathbb{R}^M \to \mathbb{R}^M$ is a family of nonsingular, nonlinear transformations. Based on the Bayesian rule, the posterior p.d.f. at a given time $t + 1$ is given by

$$(2.4) \qquad f_{t+1|t+1}(x|z_{1:t+1}) = \frac{f_{t+1}(z_{t+1}|x) f_{t+1|t}(x|z_{1:t})}{\int f_{t+1}(z_{t+1}|x) f_{t+1|t}(x|z_{1:t}) \, dx},$$

where $f_{t+1}(z|x)$ is the likelihood function associated with (2.3) and the posterior predictive distribution, $f_{t+1|t}(x|z_{1:t})$, is defined in (2.2).

REMARK 2.1. The widely-known Kalman filter is a special case of the Bayesian filtering formulation given in equation (2.4). Indeed, if one considered that ϕ_t, η_t were linear and v_t, w_t were normally distributed, then equations (2.2) and (2.4) would enjoy a closed-form solution which would be the same as in the Kalman filter.

On the other hand, our focus is on tracking multiple objects which move simultaneously. Motivated by the single object tracking framework described in equations (2.2) and (2.4), we consider *a statistical framework which allows us to generalize the prediction equation* (2.2) *and the corresponding update equation* (2.4), *both suitable for tracking one object to pertinent equations for tracking one set of objects*. We view for the first time in this biological problem the evolving collection of the organelles as a *single set-valued state*, $X_t = \{x_t^1, x_t^2, \ldots, x_t^{n_t}\} \in \mathcal{F}(\mathbb{R}^N)$, where n_t represents the number of objects at time t, and $\mathcal{F}(\mathbb{R}^N)$ is the collection of all finite subsets of $\mathbb{R}^N$. Similarly, the collection of experimental microscopy measurements at time t is viewed as a *single set-valued observation*, $Z_t = \{z_t^1, z_t^2, \ldots, z_t^{m_t}\} \in \mathcal{F}(\mathbb{R}^M)$, where m_t is the number of generated measurements at time t. Based on equation (2.3), each member $z_t^i \in Z_{t+1}$ is a noisy perturbation of the true state x of an organelle j at time t, where i is not necessarily equal to j.

Furthermore, the randomness in this multi-object framework is represented by modeling multi-object states, Δ_t, and multi-object measurements, M_t, as random finite sets (RFS) on the single-object state and observation spaces, $\mathbb{R}^N$ and $\mathbb{R}^M$,

respectively. The corresponding multi-object dynamics and observations are described below.

Given a realization, X_t, of the RFS, Δ_t, at time t, the multi-object state at time $t + 1$ is modeled by the RFS,

$$(2.5) \qquad \Delta_{t+1} = \left\{ \bigcup_{x \in X_t} S_{t+1|t}(x) \right\} \cup B_{t+1},$$

where $S_{t+1|t}$ is the RFS representing the objects which survive with probability $p_{S,t+1|t}(x)$, from the previous time t, and B_t is the RFS which represents the objects which enter the scene at time $t + 1$ ("newborn" organelles). Hence, the RFS, Δ_{t+1}, includes all information of set dynamics, such as the number of objects that vary over time and an individual organelle's motion [see equation (2.1)] and birth/death. Now, given a realization X_{t+1} of Δ_{t+1} at time $t + 1$, the multi-object measurements are modeled via the following RFS,

$$(2.6) \qquad M_{t+1} = \bigcup_{x \in X_t} \Theta_{t+1}(x),$$

where $\Theta_{t+1}(x)$ is the RFS of measurements generated by the object $x \in X_t$. The RFS M_{t+1} encapsulates all characteristics of the measurements from the microscopy image, for example, measurement noise.

Next, let $f_{t|t}(X'|Z_{1:t})$ denote the multi-object posterior density at a given time step t conditioned on the observation sets, $Z_{1:t} \doteq \{Z_1, Z_2, \ldots, Z_t\}$. The multi-object Bayes filter propagates the multi-object filtering distribution via the following recursion:

$$(2.7) \qquad f_{t+1|t}(X|Z_{1:t}) = \int f_{t+1|t}(X|X') f_{t+1|t}(X'|Z_{1:t}) \delta X',$$

$$(2.8) \qquad f_{t+1|t+1}(X|Z_{1:t+1}) = \frac{f_{t+1}(Z_{t+1}|X) f_{t+1|t}(X|Z_{1:t})}{\int f_{t+1}(Z_{t+1}|X) f_{t+1|t}(X|Z_{1:t}) \delta X},$$

where $\int \delta X$ is the set integral [see, e.g., Goodman, Mahler and Nguyen (1997), Definition 10], $f_{t+1|t}(X|X')$ is the multi-object transition density associated with the dynamics given in equation (2.5), and $f_{t+1}(Z_{t+1}|X)$ is the multi-object likelihood obtained by equation (2.6). One may show that densities and likelihoods expressed in equations (2.7) and (2.8) are well defined using techniques of finite set statistics (FISST) and extending the concept of the Radon–Nikodym derivative [Goodman, Mahler and Nguyen (1997), Chapter II.5].

REMARK 2.2. One may compare the analogy between equations (2.7), (2.8) and equations (2.2), (2.4), respectively. Therefore, our statistical framework generalizes the problem from tracking a single object to tracking a single set.

However, the multi-object filter described in equations (2.7) and (2.8) is intractable in most applications and the Cardinalized Probability Hypothesis Density (CPHD) approximation is considered. The CPHD produces estimates on the number of organelles and their states. A formal definition is below.

DEFINITION 2.1.   The CPHD filter recursively propagates the posterior cardinality distribution $p_{t|t}(n|Z_{1:t})$ on object-number n and the intensity function or Probability Hypothesis Density (PHD) $D_{t|t}(x|Z_{1:t})$. Given any region $S \subseteq \mathbb{R}^N$, the expected number of objects in S is derived by the integral $\int_S D_{t|t}(x|Z_{1:t})\,dx$. If $S = \mathbb{R}^N$, then $N_{t|t} = \int D_{t|t}(x|Z_{1:t})\,dx$ is the total expected number of objects in the scene.

The CPHD filter produces stable (low-variance) estimates of object number, as well as better estimates of the states of individual objects [Mahler (2007), Vo, Vo and Cantoni (2007)]. This gain in performance is achieved with increased computational cost. For instance, Vo, Vo and Cantoni (2007) implemented a Gaussian mixture CPHD whose algorithmic cost was of the order $\mathcal{O}(m^3 n)$, where m is the number of data points and n the number of objects of interest. However, the number of data points is large and the number of organelles is a priori unknown and varies in time. Therefore, the alternative Gaussian mixture implementation of Mahler and Maroulas (2013) is considered herein which decreases the computational cost to the order of $\mathcal{O}(mn)$. In fact, our technique is based on the experimental observation that all data are produced by the organelles and no false alarms exist. If false alarms were collected, for instance, due to human intervention, then equations (2.5) and (2.6) would need to be suitably formulated.

Before proceeding with the dynamics and Bayesian formulations as expressed in Propositions 2.1 and 2.2, respectively, we list the assumptions on which our Gaussian mixture approach to the CPHD is based.

ASSUMPTION 2.1.   Consider a realization $X_t = \{x_t^1, x_t^2, \ldots, x_t^{n_t}\}$ of the RFS, Δ_t, and the associated data collection $Z_t = \{z_t^1, z_t^2, \ldots, z_t^{m_t}\}$. The state of each organelle $x_t^i \in X_t, i = 1, \ldots, n_t$ is normally distributed given by

$$(2.9) \qquad x_t | x_{t-1} \sim N(x; F_{t-1} x_{t-1}, Q_{t-1}),$$

where F_{t-1} is the state transition matrix and Q_{t-1} is the process noise covariance. Similarly, each observation $z_t^j\, j = 1, \ldots, m_t, j \neq i$, is normally distributed according to

$$(2.10) \qquad z_t | x_t \sim N(z; H_t x_t, R_t),$$

where H_t is the observation matrix and R_t is the observation noise covariance.

ASSUMPTION 2.2. The survival probability, $p_{S,t+1|t}(x)$, of an organelle with state x at time t to be present at time $t + 1$ is state independent, that is, $p_{S,t+1|t}(x) = p_S$. The detection probability, $p_{D|t+1}(x)$, to collect an observation associated with an organelle whose state is x at a given time t, is state independent, that is, $p_{D|t+1}(x) = p_D$.

ASSUMPTION 2.3. The intensity measure of the birth RFS which encompasses the dynamics of newborn organelles is a Gaussian mixture of the form

$$(2.11) \qquad b_t(x) = \sum_{i=1}^{J_{b,t}} w_{b,t}^{(i)} N\big(x; \mu_{b,t}^{(i)}, P_{b,t}^i\big),$$

where $w_{b,t}^{(i)}, \mu_{b,t}^{(i)}, P_{b,t}^i$ are the weights, means and covariances of the mixture birth intensity and $J_{b,t}$ is the number of Gaussian components associated with the newborn organelles at a given time t.

REMARK 2.3. Assumptions 2.1–2.3 are crucial for establishing a closed form for the multi-object densities defined in equations (2.7) and (2.8). However, if the linearity of Assumption 2.1 is violated, then one could consider implementing a CPHD filter introduced by Vo, Vo and Cantoni (2007), which employs a pertinent approximation of the nonlinearities. However, Assumptions 2.1–2.3 are satisfied using our experimental data. Further discussion of this topic is delegated to Section 3.

The propositions below involve the main equations of the Gaussian mixture implementations of the CPHD filter without considering any false alarms. For presentation's sake, the time index is suppressed in the cardinality of the state sets and measurement sets in the propositions below, that is, $n_t = n$ and $m_{t+1} = m$. The reader should refer to Mahler and Maroulas (2013) and the references therein for their proofs.

PROPOSITION 2.1 (Prediction). *Assume that at a given time t, the posterior cardinality distribution, $p_{t|t}(n)$, is given and that the posterior PHD is a Gaussian mixture of the form $D_{t|t}(x) = \sum_{i=1}^{J_t} w_t^{(i)} N(x; \mu_t^{(i)}, P_t^{(i)})$, where J_t is the number of Gaussian components at t. Then the posterior predicted PHD, $D_{t+1|t}$, is also a Gaussian mixture,*

$$(2.12) \qquad D_{t+1|t}(x) = b_t(x) + D_{S,t+1|t}(x),$$

where $b_t(x)$ is given in (2.11) and $D_{S,t+1|t}(x) = p_S \sum_{i=1}^{J_t} w_t^{(i)} N(x; \mu_{S,t+1|t}^{(i)},$ $P_{S,t+1|t}^{(i)})$ is the PHD which arises from the "survived" organelles. The corresponding mean and covariance equal $\mu_{S,t+1|t} = F_t \mu_t$ and $P_{S,t+1|t} = Q_t + F_t P_t F_t^T$,

respectively. The posterior predictive cardinality distribution is

$$(2.13) \quad p_{t+1|t}(n|Z_{1:t}) = \sum_{j=0}^{n} p_B(n-j) \sum_{l=j}^{\infty} \binom{l}{j} p_S^j (1-p_S)^{l-j} p_{t|t}(l),$$

where $p_B(\cdot)$ is the cardinality distribution of the RFS responsible for the organelles' appearance and p_S is the survival probability of an organelle.

We denote the permutations $P_m^n = \frac{n!}{(n-m)!}$ with the convention that $P_m^n = 0$, if $n < m$, and we define $q_D = 1 - p_D$ the probability of not detecting an intracellular movement. Furthermore, assume that at time $t+1$, a new measurement random set, Z_{t+1}, is received with cardinality $|Z_{t+1}| = m$. Then the predicted PHD (2.12) and cardinality distribution (2.13) will be updated according to Proposition 2.2.

PROPOSITION 2.2 (Update). *Suppose that the predicted PHD, $D_{t+1|t}$, and the cardinality distribution, $p_{t+1|t}(n|Z_{1:t})$, satisfy Proposition 2.1. Then, the posterior PHD, $D_{t+1|t+1}$, at a given time $t+1$ is a Gaussian mixture, and the corresponding CPHD update equations are listed below:*

$$D_{t+1|t+1} = q_D \left[\frac{1}{\sum_{i=1}^{J_{t+1|t}} w_{t+1|t}^{(i)}} \frac{\sum_{n=m+1}^{\infty} P_{m+1}^n p_{t+1|t}(n) q_D^{n-(m+1)}}{\sum_{n=m}^{\infty} P_m^n p_{t+1|t}(n) q_D^{n-m}} \right] D_{t+1|t}(x)$$

$$(2.14)$$

$$+ p_D \sum_{z \in Z_{t+1}} \sum_{i=1}^{J_{t+1|t}} \bar{w}_{t+1|t}^{(i)}(z) N\left(x; \mu_{t+1}^{(i)}(z), P_{t+1}^{(i)}\right),$$

where

$$\bar{w}_{t+1|t}^{(i)}(z) = \frac{w_{t+1|t}^{(i)} q_{t+1}^{(i)}(z)}{\sum_{i=1}^{J_{t+1|t}} w_{t+1|t}^{(i)} q_{t+1}^{(i)}(z)},$$

$$q_{t+1}^{(i)}(z) = N\left(z; H_{t+1}\mu_{t+1|t}^{(i)}, R_{t+1} + H_{t+1}P_{t+1|t}^{(i)}H_{t+1}^T\right).$$

The mean and the covariance matrix are $\mu_{t+1}^{(i)}(z) = \mu_{t+1|t}^{(i)} + K_{t+1}^{(i)}(z - H_{t+1}\mu_{t+1|t}^{(i)})$, $P_{t+1}^{(i)} = [I - K_{t+1}^{(i)}H_{t+1}]P_{t+1|t}^{(i)}$, respectively, where $K_{t+1}^{(i)} = P_{t+1|t}^{(i)}H_{t+1}^T(R_{t+1} + H_{t+1}P_{t+1|t}^{(i)}H_{t+1}^T)^{-1}$. Furthermore, the posteriorcardinality distribution is propagated via the following equation:

$$(2.15) \qquad p_{t+1|t+1}(n) = p_{t+1|t}(n) \frac{P_m^n q_D^{n-m}}{\sum_{l=m}^{\infty} P_m^l p_{t+1|t}(l) q_D^{l-m}}.$$

REMARK 2.4. If there were only one intracellular movement during the tracking time and neither a birth nor a death of an organelle were allowed, then Propositions 2.1 and 2.2 would yield the special case of monitoring a random singleton,

that is, one organelle in our experiments. Furthermore, if the probability of detection $p_D = 1$ (thus $q_D = 0$) and there was one component in the Gaussian mixture, then equation (2.14) would yield the typical Kalman filter update equation and in this special case the matrix K would play the role of the Kalman gain matrix.

3. Results. Having established the theoretical framework, we present our biological data analysis and tracking in this section. We start with a summary of our algorithm.

Step 0: *Initialization*. The initial intensity, $D_{0|0}$, is considered as a Gaussian mixture with J_0 components. Furthermore, the initial cardinality distribution, $p_{0|0}(n)$, is considered a priori to a single object.

Step 1: *Prediction*. At time t the predicted intensity $D_{t+1|t}$ is a Gaussian mixture whose components' weights, means and covariance matrices are derived in equation (2.12). Equation (2.13) yields the corresponding posterior predictive cardinality distribution, $p_{t+1|t}(n)$.

Step 2: *Update*. At time $t + 1$, the predictions generated in Step 1 are updated based on new measurements. More precisely, the posterior PHD, $D_{t+1|t+1}$, is a Gaussian mixture whose weight, mean and covariance matrix is derived by equation (2.14). The posterior cardinality distribution, $p_{t+1|t+1}(n)$, is estimated according to equation (2.15).

Step 3: *Merging and pruning*. The number of Gaussian components increases as time progresses. In fact, at a given time, t, the Gaussian mixture will require $\mathcal{O}(J_{t-1}|Z_t|)$ components, where J_{t-1} is the number of components of the posterior intensity $D_{t-1|t-1}$ at time $t - 1$. Since components with low weight do not provide any significant contribution to the approximation of the posterior multi-target density, we eliminate the components whose weights are negligible and below some preset threshold, T (e.g., $T = 10^{-5}$). The remaining components of the mixture are renormalized such that their sum equals 1.

Furthermore, there are components which are close to each other and practically could be approximated by a single Gaussian distribution. Indeed, if two components of the mixture with weight, state and covariance, (w_i, x_i, P_i) and (w_j, x_j, P_j), respectively, have distance $d_{i,j} \doteq (x_i - x_j) P_i^{-1} (x_i - x_j)^t$ less than some threshold, U, then these mixing components are merged into one [Clark, Panta and Vo (2006)]. The threshold U should be chosen much smaller (e.g., $U = 0.004$) than the standard deviation of the observations' noise so that the filtering algorithm does not consider two different objects as one when they are close together, such as when their paths are crossing each other.

Step 4: *Multi-object state extraction*. To extract the organelles' states, we focus on only the modes of the corresponding Gaussian mixture. The number of organelles is estimated from the cardinality distribution using a maximum a posteriori (MAP) estimator $\hat{n} = \arg \sup_n p(n|Z_{1:t})$.

Schematically, the algorithm works in the following way, for all $t = 0, 1, \ldots$:

$$(D_{t|t}, p_{t|t}) \xrightarrow{\text{Proposition 2.1}} (D_{t+1|t}, p_{t+1|t}) \xrightarrow{\text{Proposition 2.2}} (D_{t+1|t+1}, p_{t+1|t+1}),$$

where the PHD, $D_{\cdot|\cdot}$, is estimated via the triplet of weights, mean and covariance.

3.1. *Synthetic data.* This section illustrates a simulated scenario with respect to organelle movements. Consider a set $X_t = \{x_t^1, x_t^2, \ldots, x_t^{n_t}\}$ whose members are 4-dimensional state vectors of the n_t organelles at time t. Precisely, an organelle's state vector is $x_t^i \doteq [p_{x,t}, v_{x,t}, p_{y,t}, v_{y,t}]^T$ for any $i = 1, \ldots, n_t$, where $(p_{x,t}, p_{y,t})$ denote the spatial coordinates of the organelle on the xy-plane and the corresponding velocities are denoted as $(v_{x,t}, v_{y,t})$. The movements in a cell may be considered to take place in a force field which is on average inactive. However, when a molecular motor exerts a pushing force on an organelle, then there is a positive deviation from the mean zero. By the same token, when friction and/or other large enough backward-acting forces occur, then the organelles will slow down and eventually stop, and thus a symmetric negative deviation from the mean-zero force field is caused. Therefore, one may consider that the force field is normally distributed with mean zero and pertinent covariance. This consideration is actually validated in Section 3.2 where experimental data are analyzed. Given that the mass is conservative over time frames considered here (a valid assumption), Newton's second law yields that the acceleration, a, follows a normal distribution. The velocity changes in turn are also normally distributed where the covariance depends on the size of the time intervals. Given the fact that $\dot{p}_{x,t} = v_{x,t}$ and $\dot{p}_{y,t} = v_{y,t}$, we can formally state the following linear stochastic differential equations system:

$$(3.1) \quad \begin{pmatrix} dp_{x,t} \\ dv_{x,t} \\ dp_{y,t} \\ dv_{y,t} \end{pmatrix} = \begin{pmatrix} v_{x,t} \\ 0 \\ v_{y,t} \\ 0 \end{pmatrix} dt + \begin{pmatrix} 0 & 0 \\ \sigma_x & 0 \\ 0 & 0 \\ 0 & \sigma_y \end{pmatrix} \begin{pmatrix} du_{x,t} \\ du_{y,t} \end{pmatrix},$$

where $u_{x,t}, u_{y,t}$ are independent Brownian motions and the driving noises $\sigma_x \dot{u}_{x,t}$ and $\sigma_y \dot{u}_{y,t}$ are Gaussian noises with covariances $\sigma_x^2 \delta(t)$ and $\sigma_y^2 \delta(t)$, respectively, where $\delta(t)$ is the delta function. Discretizing and approximating the system (3.1), we have a two-dimensional model given below:

$$(3.2) \quad \begin{pmatrix} p_{x,t} \\ v_{x,t} \\ p_{y,t} \\ v_{y,t} \end{pmatrix} = \begin{pmatrix} 1 & \Delta & 0 & 0 \\ 0 & 1 & 0 & 0 \\ 0 & 0 & 1 & \Delta \\ 0 & 0 & 0 & 1 \end{pmatrix} \begin{pmatrix} p_{x,t-1} \\ v_{x,t-1} \\ p_{y,t-1} \\ v_{y,t-1} \end{pmatrix} + \begin{pmatrix} \frac{\Delta^2}{2} & 0 \\ \Delta & 0 \\ 0 & \frac{\Delta^2}{2} \\ 0 & \Delta \end{pmatrix} \xi_{t-1},$$

where the model noise, ξ_{t-1}, is a collection of independent Gaussian random variables with covariance matrix $\Sigma = \mathrm{diag}\{\sigma_x^2, \sigma_y^2\}$. The sampling time is considered $\Delta = 1$ s since data from organelles' movements are collected every one second. The velocity changes are normally distributed with mean zero, and thus 99.7% of the data are within three standard deviations from zero. Taking into

consideration the biological finding that organelles may move up to 7 μm/s (in both directions) [Tominaga et al. (2003)], the standard deviation coefficients are chosen $\sigma_x = \sigma_y = 2.33$ μm/s^2. If one decreased or increased drastically the variance, then the estimates would not be accurate. Small noise dynamics (e.g., $\sigma_x = \sigma_y = 0.1$ μm/s^2) yield predictions based on almost perfect linear dynamics which could lead to erroneous estimation in case organelles exhibit a slightly curvy behavior. By the same token, a large standard deviation (e.g., $\sigma_x = \sigma_y = 5$ μm/s^2) produces a wide range of samples which lead to inaccurate estimates.

Furthermore, each object is considered with survival probability, $p_{S,t} = 0.99$, such that any organelle within the tracking domain is under monitoring unless its signal disappears. The maximum number of involved Gaussian components is considered to be fairly large, $N_{\max} = 200$. The object-birth process is a Poisson RFS with intensity defined as in (2.11), where $w_b = 0.25$, $\mu_b^{(1)} = [3\ 0\ 5\ 0]^T$, $\mu_b^{(2)} = [4\ 0\ -6\ 0]^T$, $\mu_b^{(3)} = [-3\ 0\ -2\ 0]^T$, $\mu_b^{(4)} = [-4\ 0\ 8\ 0]^T$, and $P_b = 10\mathbb{I}_4$. The four different means, $\mu_b^{(i)}$, $i = 1, \ldots, 4$ are selected to ensure that births on all four quadrants are considered with equal probability $w_b = 0.25$. The covariance of the birth intensity is also large such that a vast candidate area of newborn organelles is covered. Given that our experimental environment did not suffer from low signal-to-noise ratio and no false alarm occurred, the probability of detecting an organelle is state independent and equals $p_{D,t} = 0.98$.

We first focus on the synthetic data which consist of the spatial coordinates. Consider at given time $t + 1$ the random set, $Z_{t+1} = \{z_{t+1}^1, z_{t+1}^2, \ldots, z_{t+1}^{m_{t+1}}\}$, where for each i the data $z_{t+1}^i = (p_{x,t+1}, p_{y,t+1})$, $i = 1, \ldots, m_t$, is a two-dimensional vector whose likelihood is defined in (2.10), with

$$(3.3) \qquad H_t = \begin{pmatrix} 1 & 0 & 0 & 0 \\ 0 & 0 & 1 & 0 \end{pmatrix}, \qquad R_t = \sigma_o^2 \mathbb{I}_2,$$

and $\sigma_o = 0.2$ μm is the standard deviation of the measurement noise due to optical limitations and experimental noise. For example, there is a fundamental maximum to the resolution of any optical system due to diffraction. The diffraction defines the microscope's point-spread function which describes the response of an imaging system to a point light source. Furthermore, our procedure uses a weight threshold $T = 10^{-5}$ for the pruning procedure and a threshold $U = 0.004$ for the merging part of the algorithm (step 3 in the algorithm).

The synthesized organelles' trajectories, which play the role of the true trajectories, are created by evolving a number of organelles according to dynamics (3.2), and the corresponding observations were created after perturbing the true trajectories by a normally distributed noise with covariance R_t as in (3.3).

Figure 1 shows that there are twelve organelles (in total) which are monitored for 100 time steps. At any given time t, the number of organelles is unknown a priori and is not fixed, that is, random birth and death of organelles are allowed with pertinent dynamics based on Assumption 2.3. In fact, the organelles' number
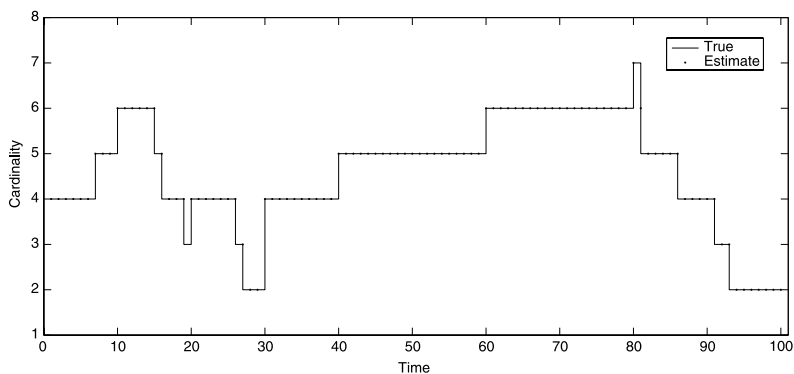
FIG. 1.   *Number of organelles per time step.*

increases and decreases drastically during the first thirty steps and the last twenty ones as well. This makes the problem a rather formidable one by keeping in mind that previous studies have monitored simultaneously a fixed and a priori known number of intracellular movements with overall known dynamics, for example, Smal, Niessen and Meijering (2006). In contrast, our algorithm assumes an initial cardinality of 1 (see step 1 of the algorithmic description) and updates its estimate based on available data. Thus, our algorithm captures accurately all modifications in the number of organelles and it gives an accurate estimate.

Figure 2 shows a three-dimensional graph of the trajectories' estimates of the organelles across time. As we can see, there are several crossings, often in the *y*-direction. Tracking methods for intracellular movements that assume one-to-one correspondence between a measurement and an object fail to resolve the most ambiguous track interaction scenarios, for example, when objects are in close prox-
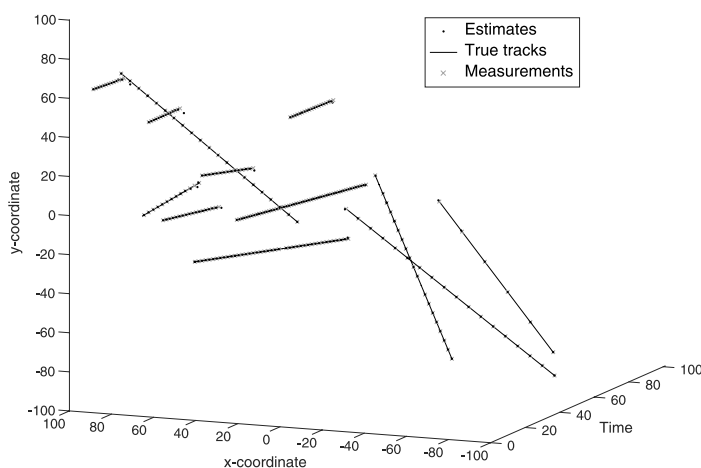

FIG. 2.   *Linear trajectories of organelles in the xy-plane over time.*

imity. However, in our case, we do not assume any sort of prior one-to-one correspondence, instead we employ a multi-object statistical framework by considering a single set of objects, thereby producing accurate estimates even during the difficult occasions such as crossings.

Indeed, the estimates are very close to the true trajectories, but to quantify any sort of error a multi-object error distance is considered. The characteristics of a multi-object distance should (1) be a metric on the space of finite sets, (2) capture cardinality and state errors and (3) have a physical interpretation. Toward this end, we employ a metric from point processes theory in order to measure the discrepancy between the estimates and the true values [Brémaud (1981), Møller and Waagepetersen (2004)]. A formal definition of this metric according to Schuhmacher, Vo and Vo (2008) is given below.

DEFINITION 3.1.   Let $W \subset \mathbb{R}^N$ be a closed and bounded observation window and d denote the Euclidean metric. For $c > 0$, let $d^{(c)}(x, y) \doteq \min(c, d(x, y))$ denote the distance between $x, y \in W$ and P_n denote the set of permutations on $\{1, 2, \ldots, n\}$ for any $n \in \mathbb{N}$. For $1 \leq \ell < \infty, c > 0$ and arbitrary finite subsets $X = \{x_1, \ldots, x_m\}$ and $Y = \{y_1, \ldots, y_n\}$ of W, where $m, n = 0, 1, 2, \ldots$, define for $m \leq n$,

$$(3.4) \qquad \bar{d}_\ell^{(c)}(X, Y) \doteq \left(\frac{1}{n} \left(\min_{\pi \in P_n} \sum_{i=1}^m d^{(c)}(x_i, y_{\pi(i)})^\ell + c^\ell (n - m) \right) \right)^{1/\ell},$$

and $\bar{d}_\ell^{(c)}(X, Y) = \bar{d}_\ell^{(c)}(Y, X)$ if $m > n$. Moreover, if $\ell = \infty$, then

$$\bar{d}_\infty^{(c)}(X, Y) = \min_{\pi \in P_n} \max_{1 \leq i \leq n} d^{(c)}(x_i, y_{\pi(i)}) \qquad \text{if } m = n$$

(3.5)

$$= c \qquad \text{if } m \neq n.$$

For any $\ell \in [1, \infty]$ the distance is equal to zero if $m = n = 0$. The function $\bar{d}_\ell^{(c)}(X, Y)$ is called the Optimal SubPattern Assignment (OSPA) metric of order ℓ with cutoff parameter c.

REMARK 3.1.   Schuhmacher and Xia (2008) examined the special case for $\ell = c = 1$ and Schuhmacher, Vo and Vo (2008) generalized it for any ℓ, c. The metric $\bar{d}_\ell^{(c)}$ is based on a Wasserstein construction. The advantage of this metric is that equation (3.4) takes into consideration the error due to localization and cardinality at the same time. An alternative measure of discrepancy is the Haussdorff distance [Møller and Waagepetersen (2004)], however, it is relatively insensitive to difference in cardinality as was noted in Hoffman and Mahler (2002). The order parameter ℓ is similar to the parameter of the ℓth order Wasserstein metric between the empirical distributions of the point patterns X and Y. Furthermore, given that c is fixed, the parameter ℓ in (3.4) assigns more weight to outliers.
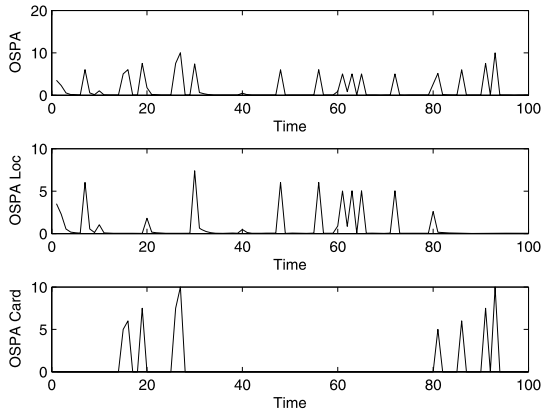
FIG. 3. *Error measured via the OSPA metric. The error can be as large as the cutoff parameter* $c = 30$.

The metric $\bar{d}_\ell^{(c)}(X, Y) \in [0, c]$ for any $c > 0$ in turn gives us a measure of performance with respect to the worst possible distance ℓ. Also, if $0 < c_1 < c_2 < \infty$, then $\bar{d}_\ell^{(c_1)} \leq \bar{d}_\ell^{(c_2)}$. Moreover, the cutoff parameter c determines the weighting of how the metric penalizes cardinality errors as opposed to localization errors. Smaller values of c tend to put emphasis on the localization error and make the metric unchanged by cardinality errors. Thus, the designer can determine how strongly a false or missing estimate will be penalized by modifying the value of c. Here, we have chosen $\ell = 1$ and $c = 30$ such that the OSPA is sensitive enough in both localization and cardinality errors. The choice of the value $\ell = 1$ has the benefit that the OSPA-metric measures a first order per-object error and that the sum of localization and cardinality components equals the total metric. The reader should refer to Schuhmacher, Vo and Vo (2008) and the references therein for further details on the OSPA metric.

The top picture in Figure 3 depicts the error using the OSPA metric given in equation (3.4). We observe that large errors (peaks in the figure) occur when the organelles are crossing and when there is a change of the number of organelles (e.g., at $t = 20$). This is expected since these are the most difficult situations. The OSPA error cannot exceed the value 30 since the cutoff parameter is set at $c = 30$, however, even in the most difficult cases, the error remains well below 10. The two subsequent pictures are showing localization and cardinality error. The localization errors for two patterns $X = (x_1, \ldots, x_m)$ and $Y = (y_1, \ldots, y_n)$ with $m \leq n$ and $\ell < \infty$ are given by

$$\bar{e}_{\ell,\text{loc}}^{(c)}(X, Y) = \left(\frac{1}{n} \left(\min_{\pi \in P_n} \sum_{i=1}^{m} d^{(c)}(x_i, y_{\pi(i)})^\ell \right) \right)^{1/\ell},$$
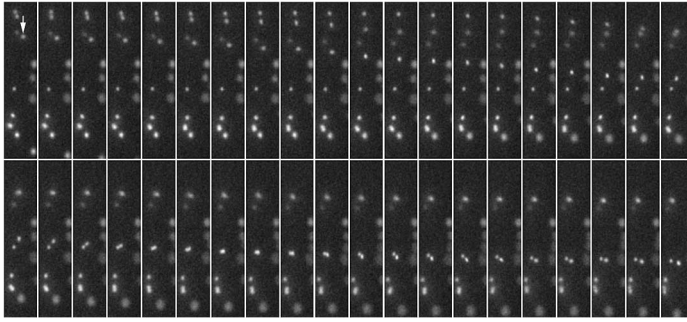
FIG. 4.   *Peroxisomes movements.*

$$\bar{e}_{\ell,\text{card}}^{(c)}(X, Y) = \left(\frac{c^{\ell}(n - m)}{n}\right)^{1/\ell}.$$

Strictly speaking, the two errors, $\bar{e}_{\ell,\text{loc}}^{(c)}$ and $\bar{e}_{\ell,\text{card}}^{(c)}$, are not metrics on the space of finite subsets, but one may still gain some insight about the performance of the filter [Schuhmacher, Vo and Vo (2008)].

3.2. *Experimental data.*   Before outlining our results, we will briefly describe the conditions under which the movement data were retrieved. Organelles were labeled with fluorescent protein fusions in root cells of the model plant *Arabidopsis thaliana* and cells on the surface of roots were observed on a fluorescent microscope as described in Nelson, Cai and Nebenführ (2007). Images were taken with a digital camera at regular intervals (1 s) to generate time-lapse sequences of 1 to 2 minute duration (i.e., 60 to 120 images). These image sequences (e.g., Figure 4) displayed bright spots of different sizes and intensities depending on the size and position of the organelle relative to the focal plane. Movements of individual organelles were readily apparent by comparing the changes in position of spots between image frames (arrow in Figure 4). Specifically, Figure 4 shows the movement of peroxisomes, small spherical organelles involved in detoxification of reactive oxygen species which have recently emerged as important regulators of plant growth and stress responses [Klaus and Heribert (2004)]. Similar movements can also be observed for other organelles, such as Golgi stacks [Nebenführ et al. (1999)] and mitochondria [Van Gestel, Köhler and Verbelen (2002)].

Images were analyzed quantitatively by manually marking the center of each spot in every frame of the time-lapse sequence which was then recorded by the Manual Tracking plugin in ImageJ [Schneider, Rasband and Eliceiri (2012)]. This procedure produced a series of (x, y) coordinates per image frame that were manually linked to specific (x, y) coordinates in subsequent frames. The procedure of manually linking is typically slow (about 1 hour for the data set that is analyzed herein) and bias due to human decision in linking can be a frequent disadvantage. In our case, the resulting two-dimensional vectors declaring the position of

Acceleration	*p*-value	H_0
a_x	0.31	Accept
a_y	0.3265	Accept

organelles on the xy-plane at every time point were used (1) to calculate the instantaneous velocities of the organelles over time; (2) to provide experimental values for the accelerations' distributions; and (3) to provide the raw data to the statistical tracking algorithm without knowing a priori which data (coordinates) correspond to which organelle.

In the following, we focus on the motions of eight peroxisomes retrieved in experiments in the second author's lab. First, we decompose the acceleration, and we investigate the distributional behavior of the accelerations per coordinate separately based on the experimental data. There are $m = 284$ acceleration data points from the eight peroxisomes with mean and standard deviation on the x-axis, $\mu_x^a = -0.0326$, $\sigma_x^a = 0.9998$, respectively. The corresponding mean and standard deviation on the y-axis are $\mu_y^a = 0.0429$, $\sigma_y^a = 0.6922$. Next, we test if the accelerations follow a normal distribution using a Kolmogorov–Smirnov test and visually by plotting two normality plots, one per coordinate. As we can see from the results of the Kolmogorov–Smirnov tests presented in Table 1, and the normal probability plots in Figure 5, the two accelerations of the eight peroxisomes follow a Gaussian distribution. Thus, the arguments of Section 3.1 imply that the dynamics of the eight peroxisomes can be described by the discrete system in (3.2).
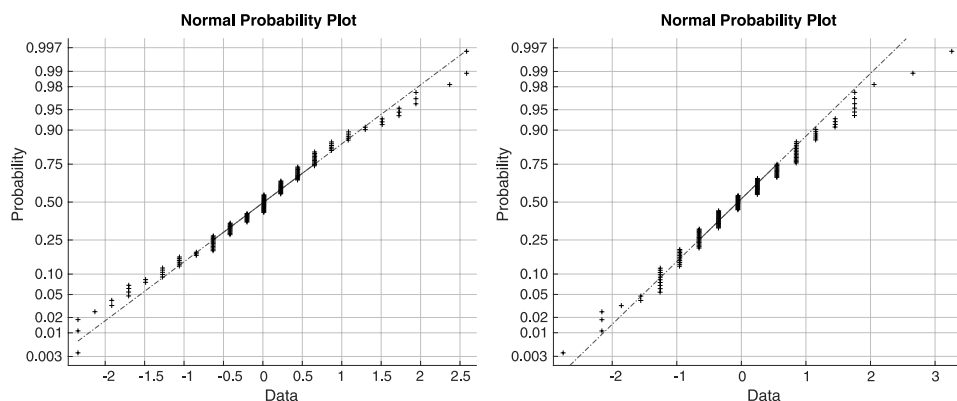

FIG. 5. *Testing normality of the organelles' acceleration.* Left panel: *Acceleration on the x-axis.* Right panel: *Acceleration on the y-axis.*
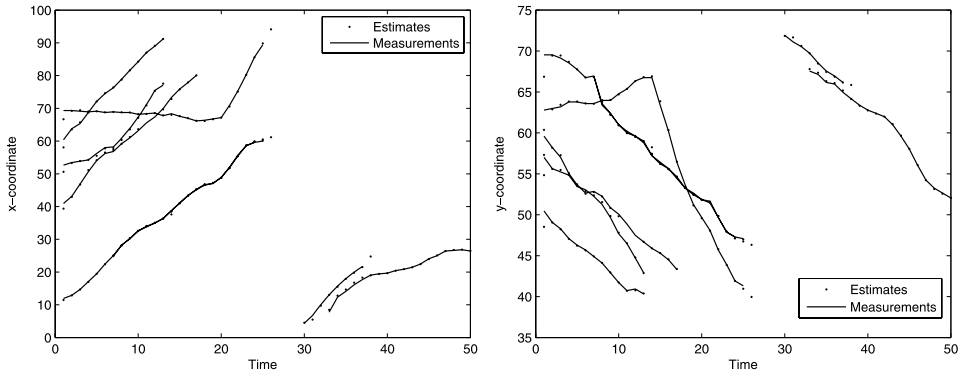
FIG. 6.   *Trajectories of organelles*. Left panel: *Trajectories in the x-direction*. Right panel: *Trajectories in the y-direction*.

Therefore, employing the dynamics (3.2) accompanied by the several hyperparameters discussed in Section 3.1, we describe our findings for the motions of the peroxisomes. Figures 6 and 7 show the trajectories based on measurements (line) and the corresponding estimates represented as dots in the figures. At the initial time step, Figure 6 shows a greater mismatch between the estimates and the data than in the next sampling periods. This is expected since the algorithm attempts to "learn" the pattern of the organelles' motion. Although the peroxisomes' overall trajectories are not linear, they are piecewise linear per time step (1 s), and thus the dynamics of Section 3.1 perform satisfactorily since sampling occurs every $\Delta = 1$ s. If the piecewise linearity was violated and/or the acceleration distribution
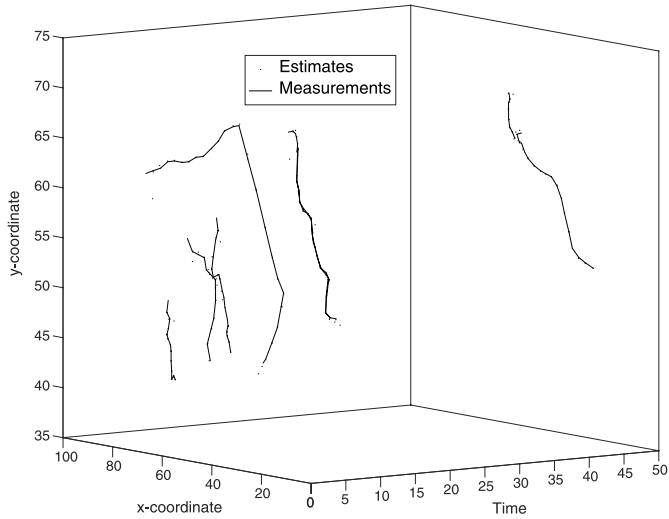

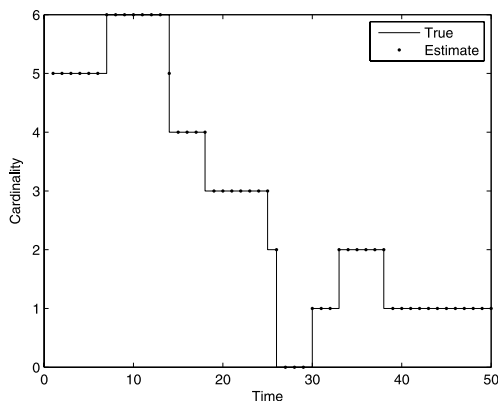FIG. 7.   *Trajectories of organelles in the xy-plane over time.*

FIG. 8. *Number of organelles per time step.*

was heavy tailed, then the dynamics in equation (3.2) would produce errors which would depend on the curvature of the true trajectories and/or the non-Gaussian noise. Figure 8 depicts the cardinality (number of peroxisomes) per time step. As we observe, the CPHD filter accurately captures the target number when their number does not vary, and it takes 1 to 2 sampling time steps to realize the change in the organelle number. Also, the algorithm correctly estimates that there were not any organelles to monitor during the time interval [26, 29]. The duration of the automated tracking process based on our algorithm is about 10 s versus roughly 1 hr for the manual tracking of the same eight peroxisomes.

Due to lacking the true trajectories of the organelles (in fact, it is impossible to know them with the current technology) [Smal, Niessen and Meijering (2006)], the OSPA measurement of error (and any other metric of this type) cannot be used since it measures the discrepancy between the algorithmic estimates and the true trajectories (not the observed measurements). However, according to our simulation results exposed in Section 3.1, we believe that our estimates are very close to the true trajectories of the eight peroxisomes.

4. Summary and discussion. In this paper we have considered the motion of organelles as evolving sets. This succeeded by incorporating random sets techniques for multi-object tracking and using the cardinalized probability hypothesis density filter. Employing a novel Gaussian mixture implementation of the CPHD filter, we were able to successfully generate an automated method for a quantitative analysis of intracellular movements, which took about 10 seconds versus about 1 hour for manually linking the same data. The new approach's computational cost was linearly dependent on the number of objects multiplied by the number of data points. Our model was capable of simultaneously monitoring a large number of organelles, specifically peroxisomes, and distinguishing them even when they were in close proximity. Consequently, not only did our algorithm monitor

the organelles but it also gave an accurate estimate on the number of organelles without assuming a fixed and known number of them. Furthermore, our data analysis revealed that the acceleration of the peroxisomes are mean-zero normally distributed, which according to Newton's second law supports an on average "inactive" force field within a cell where positive (pushing force by the myosin motors) or backward-acting forces (e.g., friction) are developed in a symmetric fashion given that mass is conservative. Consequently, the two parameters, myosin power and local friction, were fairly constant on average over time and space, respectively. On the other hand, large changes in velocity (if any) presumably would result from a static organelle engaging with a cytoskeletal track, or from a moving organelle dropping from a cytoskeletal track. We expect these changes to occur nearly instantaneously, however, technical limitations prevented us from detecting these very rapid changes if they indeed existed. In particular, we had to employ exposure times up to 100 ms to obtain sufficient signal for organelle detection. In addition, images were taken in 1 s intervals and had a nominal resolution of 200 nm per pixel. Given that myosin motors take 35 nm steps and can move up to 7 μm/s, that is, one step every 5 ms, as noted in Tominaga et al. (2003), it is apparent that these imaging parameters do not allow us to capture the anticipated very fast acceleration and deceleration events directly. Instead we can only compute the integrated behavior of organelles over many individual myosin steps. Therefore, this scientific conjecture regarding changes in organelle velocities should be further examined on large experimental data sets which could yield a more detailed distribution of accelerations, dynamics and thus potentially the mechanics within a cell overall.

Focusing on the algorithm itself, although it captures the organelles' behavior accurately, it did not take other scenarios into consideration which would increase the already severe complexity of the problem. For example, there might be cases where organelles may move in a more erratic fashion. In this scenario, the acceleration distribution might not be normally distributed and thus nonlinear and/or nonGaussian dynamics could be fruitful for such data. A possible future research avenue is to use high noise with suitably controlled drift dynamics or a more complex autoregressive model. Another way is to approximate the overall nonlinearities and/or add more experimental features, for example, include information about the shape and signal intensity of organelles in the linking step [Sbalzarini and Koumoutsakos (2005), Smal (2009), Smal, Niessen and Meijering (2006), Smal et al. (2008)]. Moreover, the organelles' survival and detection probabilities were presumed state independent and time invariant. On the other hand, these probabilities clearly depend on the position of organelles in a cell. For instance, organelles in close proximity to each other may not be detected or, given the curvature of cells, the survival probability of an organelle will decrease as it approaches an out-of-focus region of the cell. In our experimental data, crossings occurred only a few times and organelles were always in-focus and "disappeared" when they exited the focal domain. Attempting to bypass Assumption 2.2, techniques developed in

Hughes and Fricks (2011), Hughes, Fricks and Hancock (2010) may be fruitful for these difficult scenarios.

In conclusion, this manuscript offers the establishment of a systematic way of creating an automated algorithm for monitoring motility within a cell by considering a unifying statistical framework for multiple objects. In turn, such an automated tracking algorithm will greatly strengthen the study of motion patterns in cells. Consequently, understanding the typical behavior of healthy molecular processes will have a great impact in quickly recognizing abnormalities associated with disorders.

REFERENCES

AVISAR, D., PROKHNEVSKY, A. I., MAKAROVA, K. S., KOONIN, E. V. and DOLJA, V. V. (2008). Myosin XI-K is required for rapid trafficking of Golgi stacks, peroxisomes, and mitochondria in leaf cells of Nicotiana benthamiana. *Plant Physiol*. **146** 1098–1108.

BAR-SHALOM, Y. and BLAIR, W. D. (2000). *Multitarget-Multisensor Tracking*: *Applications and Advances*. Norwood, MA, Artech House.

BLACKMAN, S. and POPOLI, R. (1999). *Design and Analysis of Modern Tracking Systems*. Artech House, Norwood, MA.

BRÉMAUD, P. (1981). *Point Processes and Queues*: *Martingale Dynamics*. Springer, New York. MR0636252

CLARK, D. E., PANTA, K. and VO, B.-N. (2006). The GM-PHD filter multiple target tracker. In 9*th International Conference on Information Fusion* 1–8. IEEE.

COLLINGS, D. A., HARPER, J. D. I., MARC, J., OVERALL, R. and MULLEN, L. R. T. (2002). Life in the fast lane: Actin-based motility of plant peroxisomes. *Canadian Journal of Botany* **80** 430–441.

CORTI, B. (1774). *Osservazioni microscopiche sulla tremella e sulla circolazione del fluido in una pianta acquajuola*. Lucca.

DALEY, D. J. and VERE-JONES, D. (1988). *An Introduction to the Theory of Point Processes*. Springer, New York. MR0950166

DANUSER, G. (2011). Computer vision in cell biology. *Cell* **147** 973–978.

DOUCET, A., DE FREITAS, N. and GORDON, N., eds. (2001). *Sequential Monte Carlo Methods in Practice*. Springer, New York. MR1847783

FORTMANN, T. E., BAR-SHALOM, Y. and SCHEFFE, M. (1983). Sonar tracking of multiple targets using joint probabilistic data association. *Oceanic Engineering*, *IEEE Journal of* **8** 173–184.

GILKS, W. R. and BERZUINI, C. (2001). Following a moving target—Monte Carlo inference for dynamic Bayesian models. *J. R. Stat. Soc. Ser. B. Stat. Methodol*. **63** 127–146. MR1811995

GOODMAN, I. R., MAHLER, R. P. S. and NGUYEN, H. T. (1997). *Mathematics of Data Fusion*. *Theory and Decision Library. Series B*: *Mathematical and Statistical Methods* **37**. Kluwer Academic, Dordrecht. MR1635258

GORDON, N. J., SALMOND, D. J. and SMITH, A. F. M. (1993). Novel approach to nonlinear/non-Gaussian Bayesian state estimation. *Radar and Signal Processing*, *IEE Proceedings F* **140** 107–113.

GUTIERREZ, R., LINDEBOOM, J. J., PAREDEZ, A. R., EMONS, A. M. C. and EHRHARDT, D. W. (2009). Arabidopsis cortical microtubules position cellulose synthase delivery to the plasma membrane and interact with cellulose synthase trafficking compartments. *Nature Cell Biology* **11** 797–806.

HAMADA, T., TOMINAGA, M., FUKAYA, T., NAKAMURA, M., NAKANO, A., WATANABE, Y., HASHIMOTO, T. and BASKIN, T. I. (2012). RNA processing bodies, peroxisomes, golgi bodies, mitochondria, and endoplasmic reticulum tubule junctions frequently pause at cortical microtubules. *Plant and Cell Physiology* **53** 699–798.

HOFFMAN, J. R. and MAHLER, R. P. S. (2002). Multitarget miss distance and its applications. In *Proceedings of the Fifth International Conference on Information Fusion* 1 149–155. IEEE.

HUGHES, J. and FRICKS, J. (2011). A mixture model for quantum dot images of kinesin motor assays. *Biometrics* **67** 588–595. MR2829027

HUGHES, J., FRICKS, J. and HANCOCK, W. (2010). Likelihood inference for particle location in fluorescence microscopy. *Ann. Appl. Stat.* **4** 830–848. MR2758423

JAQAMAN, K., LOERKE, D., METTLEN, M., KUWATA, H., GRINSTEIN, S., SCHMIDT, S. L. and DANUSER, G. (2008). Robust single-particle tracking in live-cell time-lapse sequences. *Nat. Methods* **5** 695–702.

KANG, K. and MAROULAS, V. (2013). Drift homotopy methods for a nonGaussian filter. In 16*th International Conference on Information Fusion* (*FUSION*) 1088–1094. IEEE, Istanbul.

KANG, K., MAROULAS, V. and SCHIZAS, I. D. (2014). Drift homotopy particle filter for non-Gaussian multi-target tracking. In 17*th International Conference on Information Fusion* (*FUSION*) 1–7. IEEE, Salamanca.

KLAUS, A. and HERIBERT, H. (2004). Reactive oxygen species: Metabolism, oxidative stress, and signal transduction. *Annual Review of Plant Biology* **55** 373–399.

LIU, J. S. (2008). *Monte Carlo Strategies in Scientific Computing*. Springer, New York. MR2401592

LIU, J. S. and CHEN, R. (1998). Sequential Monte Carlo methods for dynamic systems. *J. Amer. Statist. Assoc.* **93** 1032–1044. MR1649198

LOGAN, D. C. and LEAVER, C. J. (2000). Mitochondria-targeted GFP highlights the heterogeneity of mitochondrial shape, size and movement within living plant cells. *J. Experimental Botany* **51** 865–871.

MADISON, S. L. and NEBENFÜHR, A. (2013). Understanding myosin functions in plants: Are we there yet? Preprint.

MAHLER, R. P. S. (2003). Multitarget Bayes filtering via first-order multitarget moments. *Aerospace and Electronic Systems*, *IEEE Transactions on* **39** 1152–1178.

MAHLER, R. P. S. (2007). *Statistical Multisource-Multitarget Information Fusion*. Artech House, Norwood, MA.

MAHLER, R. P. S. and MAROULAS, V. (2013). Tracking spawning objects. *Radar*, *Sonar Navigation*, *IET* **7** 321–331.

MAROULAS, V. and STINIS, P. (2012). Improved particle filters for multi-target tracking. *J. Comput. Phys.* **231** 602–611. MR2872093

MØLLER, J. and WAAGEPETERSEN, R. P. (2004). *Statistical Inference and Simulation for Spatial Point Processes*. *Monographs on Statistics and Applied Probability* **100**. Chapman & Hall/CRC, Boca Raton, FL. MR2004226

NEBENFÜHR, A., GALLAGHER, L. A., DUNAHAY, T. G., FROHLICK, J. A., MAZURKIEWICZ, A. M., MEEHL, J. B. and STAEHELIN, L. A. (1999). Stop-and-go movements of plant Golgi stacks are mediated by the actomyosin system. *Plant Physiol.* **121** 1127–1141.

NELSON, B. K., CAI, X. and NEBENFÜHR, A. (2007). A multi-color set of in vivo organelle markers for colocalization studies in Arabidopsis and other plants. *Plant Journal* **51** 1126–1136.

OJANGU, E.-L., TANNER, K., PATA, P., JÄRVE, K., HOLWEG, C. L., TRUVE, E. and PAVES, H. (2012). Myosins XI-K, XI-1, and XI-2 are required for development of pavement cells, trichomes, and stigmatic papillae in Arabidopsis. *BMC Plant Biol*. **12** 81.

PAREDEZ, A. R., SOMERVILLE, C. R. and EHRHARDT, D. W. (2006). Visualization of cellulose synthase demonstrates functional association with microtubules. *Science* **311** 1491–1495.

PEREMYSLOV, V. V., PROKHNEVSKY, A. I., AVISAR, D. and DOLJA, V. V. (2008). Two class XI myosins function in organelle trafficking and root hair development in Arabidopsis. *Plant Physiol*. **146** 1009–1116.

SBALZARINI, I. F. and KOUMOUTSAKOS, P. (2005). Feature point tracking and trajectory analysis for video imaging in cell biology. *J. Struct. Biol*. **151** 182–195.

SCHNEIDER, C. A., RASBAND, W. S. and ELICEIRI, K. W. (2012). NIH image to ImageJ: 25 years of image analysis. *Nat. Methods* **9** 671–675.

SCHUHMACHER, D., VO, B.-T. and VO, B.-N. (2008). A consistent metric for performance evaluation of multi-object filters. *IEEE Trans. Signal Process*. **56** 3447–3457. MR2516955

SCHUHMACHER, D. and XIA, A. (2008). A new metric between distributions of point processes. *Adv. in Appl. Probab*. **40** 651–672. MR2454027

SHIMMEN, T. (2007). The sliding theory of cytoplasmic streaming: Fifty years of progress. *J. Plant Res*. **120** 31–43.

SHIMMEN, T. and YOKOTA, E. (1994). Physiological and biochemical aspects of cytoplasmic streaming. *International Review of Cytology* **155** 97–139.

SMAL, I. (2009). Particle filtering methods for subcellular motion analysis. Ph.D. thesis, Erasmus Univ. Rotterdam, Rotterdam, The Netherlands.

SMAL, I., NIESSEN, W. and MEIJERING, E. (2006). Particle filtering for multiple object tracking in molecular cell biology. In *IEEE Nonlinear Statistical Signal Processing Workshop* 129–132. IEEE.

SMAL, I., DRAEGESTEIN, K., GALJART, N., NIESSEN, W. and MEIJERING, E. (2008). Particle filtering for multiple object tracking in dynamic fluorescence microscopy images: Application to microtubule growth analysis. *Medical Imaging, IEEE Transactions on* **27** 789–804.

SNYDER, C., BENGTSSON, T., BICKEL, P. and ANDERSON, J. (2008). Obstacles to high-dimensional particle filtering. *Mon. Wea. Rev*. **136** 4629–4640.

TOMINAGA, M., KOJIMA, H., YOKOTA, E., ORII, H., NAKAMORI, R., KATAYAMA, E., NASON, M., SHIMMEN, T. and OIWA, K. (2003). Higher plant myosin XI moves processively on actin with 35 nm steps at high velocity. *EMBO Journal* **22** 1263–1272.

VAN GESTEL, K., KÖHLER, R. H. and VERBELEN, J.-P. (2002). Plant mitochondria move on F-actin, but their positioning in the cortical cytoplasm depends on both F-actin and microtubules. *J. Experimental Botany* **53** 659–667.

VICK, J. K. and NEBENFÜHR, A. (2012). Putting on the breaks: Regulation of organelle movements in plant cellst. *Journal of Integrative Plant Biology* **54** 868–874.

VO, B.-T., VO, B.-N. and CANTONI, A. (2007). Analytic implementations of the cardinalized probability hypothesis density filter. *IEEE Trans. Signal Process*. **55** 3553–3567. MR2517522

WEARE, J. (2009). Particle filtering with path sampling and an application to a bimodal ocean current model. *J. Comput. Phys*. **228** 4312–4331. MR2531900

DEPARTMENT OF MATHEMATICS
UNIVERSITY OF TENNESSEE
1403 CIRCLE DR.
KNOXVILLE, TENNESSEE 37996
USA
E-MAIL: vmaroula@utk.edu

DEPARTMENT OF BIOCHEMISTRY
  AND CELLULAR AND MOLECULAR BIOLOGY
UNIVERSITY OF TENNESSEE
1414 CUMBERLAND AVENUE
KNOXVILLE, TENNESSEE 37996
USA
E-MAIL: nebenfuehr@utk.edu